Rheology of Steady-State Draining Foams

Raenell Soller and Stephan A. Koehler*

Department of Physics, Emory University, Atlanta, Georgia 30322, USA

(Received 18 July 2007; published 19 May 2008)

We developed the foam drainage rheology technique in order to perform rheological measurements of aqueous foams at a set liquid fraction ϵ and fixed bubble radius R without the usual difficulties associated with fluid drainage and bubble coarsening. The shear stress exhibits a power-law dependence on strain-rate, $\tau \sim \dot{\gamma}^n$ where $n \approx 0.2$. The stress exhibits an inverse dependence on liquid content, $\tau \sim (1 + h'\epsilon)^{-1}$, where $h' = \mathcal{O}(10)$ exhibits a diminishing logarithmic trend with $\dot{\gamma}$. We propose a model based upon film shearing as the dominant source of viscous dissipation.

DOI: 10.1103/PhysRevLett.100.208301 PACS numbers: 83.80.Iz, 47.57.−s

Although foams are merely compressed bubbles, they exhibit a rich variety of mechanical and dynamical behaviors [1]. They often serve as model systems for soft or granular matter [2,3], and are used in a variety of industrial applications [4]. Understanding of the dissipation mechanisms of sheared foams remains poor [3,5], and consequently all models are semiempirical. It is well known that shear stresses diminish with increased liquid volume fractions, but to date only one rheological model [6] includes a liquid volume fraction dependence. The dominant source of viscous dissipation for shearing is assumed to be films stretching and contracting. The model predicts shear thinning, which is a sublinear power-law dependence of stress on strain rate; however, the exponent is at odds with recent measurements [3,7]. Additionally, this model does not account for surfactant chemistry, which has been shown to affect rheology [8]. On the experimental side, rheological measurements are challenging because foams age due to fluid drainage and bubble coarsening [9]. Thus despite an apparent simplicity in composition, foam mechanics continues to present challenges to theorists and experimentalists alike.

To provide additional insights into dissipation mechanisms occurring during continuous shearing, we have developed the foam drainage rheology (FDR) technique. Rather than following conventional batch methods where a foam is placed into a shear cell and subjected to a battery of rheological tests, we fix the shear rate and vary the liquid volume fraction. Thus the dependence on liquid content is directly measured on the fly, without the tedious preparation of separate foams for each liquid volume fraction. Moreover, fluid and bubbles are replenished to create an ageless foam inside the shear cell with fixed bubble size and uniform liquid content, whereas in batch processes the foam immediately starts draining and coarsening once placed into a shear cell. Our results are at odds with the film-stretching model, and instead indicate that film shearing is the dominant dissipation mechanism.

According to the film-stretching model [10,11], the main source of dissipation is due to films stretching out of and contracting into Plateau borders, see Fig. 1(a). The changing film area leads to a convergent (or dilation) flow in the transitional region at the edges of Plateau borders, see Fig. 1(b). Princen and Schwartz [12] calculated the dependence of shear stress τ on strain rate $\dot{\gamma}$ for oscillatory shear. They found $\tau \propto (T/R)\mathrm{Ca}^{2/3}$, where $\mathrm{Ca} = \mu R\dot{\gamma}/T$ is the capillary number with μ, T, and R being the fluid viscosity, surface tension, and effective bubble radius, respectively. Subsequently, Princen and Kiss [6] performed experiments on continuously sheared emulsions, which are geometrically equivalent to foams but age considerably slower. They developed a semiempirical model that combines elements of the film-stretching calculation with a yield-stress term

$$\tau = \tfrac{T}{R}[c_1(\epsilon_c - \epsilon)\mathrm{Ca}^{1/2} - (c_2 \ln(\epsilon) + c_3)(1 - \epsilon)^{1/3}], \quad (1)$$

where ϵ_c is the critical continuous fraction at which rigidity is lost and the fitting parameters are in Table I. However, Eq. (1) is at odds with rheological measurements by Rodts, Baudes, and Coussot [7] performed on a shaving cream foam. Instead they found a simple power-law (Bingham) behavior with a threshold flow criterion

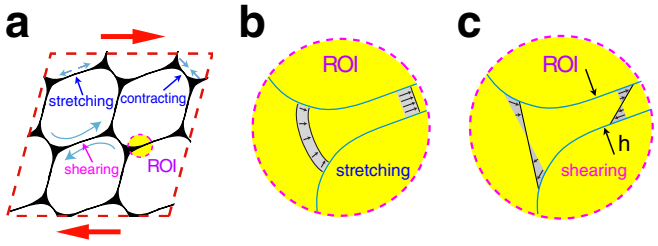

FIG. 1 (color online). (a) Schematic representation of a sheared foam showing two flow scenarios: stretching or contracting films, and film shearing. The highlighted region of interest (ROI) is the transition region between a channel and adjoining film. (b) Film stretching, where flow converges from the channel into the film. (c) Film shearing, where bubbles slide past each other on lubricating films of thickness h.

TABLE I. Parameters of the film-stretching model for emulsions [6] and optimized for foams. The last column is the mean-square error, $\langle \chi^2 \rangle = N^{-1} \sum_{i=1}^{N} (m_i/p_i - 1)^2$, where m_i and p_i are a series of measurements and predictions.

	c_1	c_2	c_3	ϵ_c	$\langle \chi^2 \rangle$
Emulsion	32	0.11	0.08	0.27	4.8×10^{-2}
Foam	144 ± 21	0.17 ± 0.03	$0.08 \pm .007$	0.36	5.2×10^{-3}

$$\tau/\tau_c \propto (\dot{\gamma}/\dot{\gamma}_c)^n \quad \text{for} \quad \dot{\gamma} \geq \dot{\gamma}_c, \tag{2}$$

with $n \approx 0.25$.

The FDR technique creates a foam with controlled liquid content and steady-state bubble size inside a wide-gap Couette geometry by liquid perfusion from above and continuous bubble generation from below. Figure 2(a) schematically shows the shear cell, where the inner cylinder is immersed into the top half of the foam to depth $Z = 9.5$ cm and rotated by a rheometer (AR2000, TA Instruments) at angular velocity ω. Bubbles are continuously and slowly injected into the fluid reservoir at the bottom, which rise at a rate of 0.1 mm/s, and are popped at the top by a hot wire loop. A 1% detergent (Dawn® by Procter & Gamble) dilution in water is chosen for good foamability, where $\mu = 0.01$ g/cm/s and $T = 20$ dynes/cm. Pictures show $R = 0.05 \pm 0.02$ cm. The rotating cylinder experiences an average shear stress, which is the ratio of the measured torque M to the surface area and radius

$$\langle \tau \rangle = \int_{z<Z} \tau dz/Z = M/\left(\frac{1}{2}\pi D_1^2 Z\right). \tag{3}$$

Foam drainage is driven by gravity $\rho \mathbf{g}$ and capillarity, which is a diffusive process that redistributes fluid from regions of high ϵ to low ϵ. The latter can be expressed as the gradient of the Laplace pressure, $\nabla(\delta^{1/2} T R^{-1} \epsilon^{-1/2})$, where $\delta = 0.312$ is a geometric constant [13]. The mean-field liquid velocity increases with the bubbles' cross-sectional area R^2 and in the case of mobile interfaces increases with the square root of the liquid content $\epsilon^{1/2}$. Thus the drainage velocity is

$$\mathbf{u} = \frac{K R^2 \epsilon^{1/2}}{\mu}\left(\rho \mathbf{g} + \frac{\delta^{1/2} T}{R} \nabla \epsilon^{-1/2}\right). \tag{4}$$

Figure 2(b) shows a simulation [14] of the foam's changing liquid volume fraction for a two-step incremental perfusion procedure, based on the node-dominated foam drainage equation [15,16]

$$\mu \frac{\partial \epsilon}{\partial t} + K R^2 \rho \mathbf{g} \cdot \nabla \epsilon^{3/2} - \frac{\delta^{1/2} K R T}{2} \nabla^2 \epsilon = 0. \tag{5}$$

Initially the foam is drained and has negligible fluid content, then is perfused at rate $q_l = 10$ ml/min for 100 sec which is subsequently increased to $q_l = 30$ ml/min. Continuous perfusion, also known as forced drainage [17], results in a traveling front whose speed is that of the fluid in the uniformly wet plateau region. Thus inside the traveling wave $\nabla \epsilon^{-1/2} = 0$ in Eq. (4), and the mean-field fluid velocity results from a force balance of viscous drag and gravity, which is

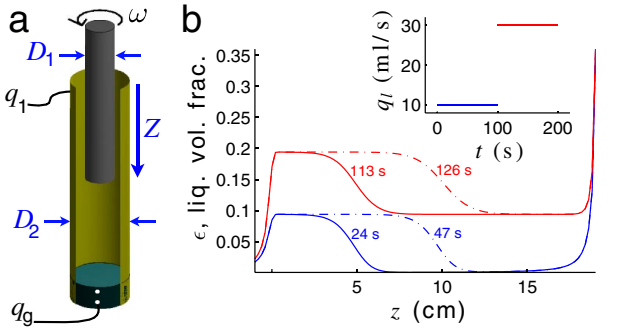

FIG. 2 (color online). (a) Schematic of the FDR apparatus. The diameters of the inner and outer cylinders are $D_1 = 1.3$ and $D_2 = 3.5$ cm, respectively. Foam is generated from the bottom by blowing N_2 gas at rate $q_g = 5$ sccm through an extra-coarse glass frits inside the surfactant fluid reservoir. The foam is perfused at rate q_l by needles located 1 cm from the top. (b) Simulation of liquid volume fraction profiles for a two-step incremental perfusion procedure, $q_l = 10,\ 30$ ml/min; the speeds of the traveling fronts are $u = 0.30,\ 0.52$ cm/sec, respectively. The inset shows the perfusion sequence.

$$u = u_0 \epsilon^{1/2}, \quad \text{with} \quad u_0 = K \rho g R^2/\mu. \tag{6}$$

Based upon previous work [15] we use $K = 3.7 \times 10^{-3}$.

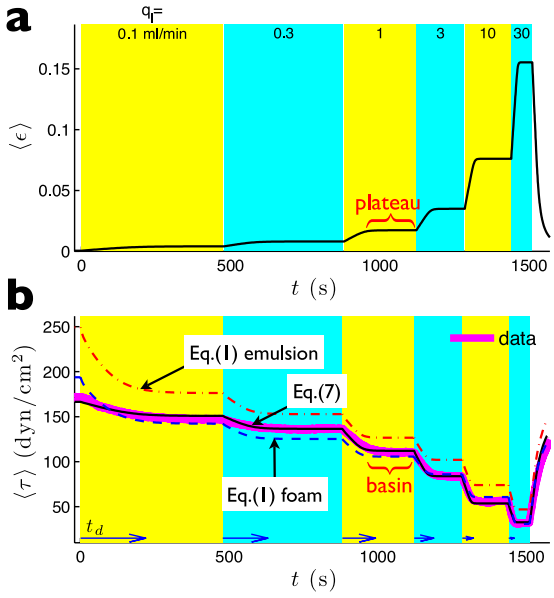

FIG. 3 (color online). Evolution of a six-step incremental perfusion, $q_l = 0.1,\ 0.3,\ 1,\ 3,\ 10,\ 30$ ml/min at $\omega = 1$ rad/s. (a) Mean liquid volume fraction; perfusion rates given at top. (b) Mean shear stress: thick magenta curve shows measurements, and three thinner curves are theoretical predictions (see text). Arrows at bottom show drainage times t_d for each step.

We found six-step sequences spanning over two decades in perfusion rates effective for determining the liquid volume fraction dependence of the stresses. Figure 3(a) shows the time evolution of the mean liquid content for the foam inside the shear gap using foam drainage theory, Eq. (5). In each perfusion step $\langle\epsilon\rangle$ increases and achieves a higher plateau value once the drainage front moved below the inner cylinder, leaving behind a uniformly wet region—see Fig. 2(b). The thick line in Fig. 3(b) shows the measured stress, which drops to lower basins for each successive perfusion. The characteristic time for the stress to achieve a 90% drop, denoted by t_d and indicated by arrows, diminishes with increasing perfusion rates because the drainage velocity grows with the perfusion rate.

We determine the drainage rates based solely upon the assumption that shear stresses monotonically decrease with liquid volume fraction. The stress drops from incremental perfusions are self-similar and rescaling by the characteristic times t_d results in their collapse onto a master curve—see Fig. 4(a). These times provide an estimate for the drainage speed, which is the distance for the drainage front to travel through the gap $u = Z/t_d$. They also provide an estimate for the liquid volume fraction, which is the ratio of the volume of the perfused fluid to that of the foam inside the gap $\epsilon = q_l t_d/\{Z\pi[(D_2/2)^2 - (D_1/2)^2]\}$. The dashed line of Fig. 4(b) shows the predicted velocity dependence using Eq. (4), which is in general agreement with the data. Thus, the $u - \epsilon$ drainage estimates, which are obtained from rheology without *a priori* knowledge of the constitutive relations conform to node-dominated foam drainage theory, which was determined by optically tracking the front of the drainage wave [15].

Having confirmed that node-dominated foam drainage theory is applicable to our experiments, we test the film-stretching model. The stress is computed from Eq. (1) using the liquid volume fraction shown in Fig. 3(a). Its average is determined using Eq. (3) and plotted as a dotted curve with dashes in Fig. 3(b), which is surprisingly close to the measurements when considering that constants for emulsions were used. These differ significantly from foams: (i) droplets are about 20 times smaller than bubbles, (ii) surface tension is about 10 times smaller, and (iii) the dispersed phase is significantly more viscous for emulsions (paraffin oil droplets vs gas bubbles). Additionally, Saint-Jalmes and Durian [9] determined that the critical liquid volume fraction at which foam loses rigidity is $\epsilon_c = 0.36$ and not 0.27. Thus, we optimize the three parameters of the film-stretching model, c_1, c_2, c_3, to provide a better fit for foams—see the dashed curve in Fig. 3(b). Although the fitting error has dropped almost tenfold cf. Table I, the curve still does not agree well with the data. Given that three free parameters were used in the optimization, the unsatisfactory agreement of the model with the data casts doubt on its general validity.

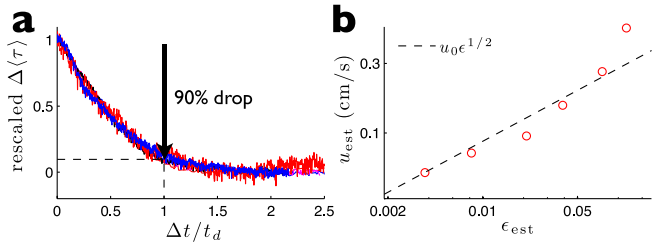

FIG. 4 (color online). (a) Rescaling of the shear stress drops using the rescaled time $\Delta t/t_d$. The inset gives the dependence of the estimated drainage velocity Z/t_d on liquid content, and the solid line is the prediction $u = 0.9\epsilon^{1/2}$ cm/s. (b) Relationship of the estimates for drainage velocity and liquid content.

Our findings join previous studies [7,8] that also are at odds with the film-stretching model. However, we use a different modeling approach based upon the liquid content dependence of the stresses afforded by FDR experiments. We reexamine the film-shearing model [5,18], which is an older model that has not received much attention because it yielded neither shear-thinning behavior nor a liquid content dependence of the stresses. As the name implies, the dominant dissipation mechanism is a lubrication flow caused by shearing bubbles inside the films with thickness h—see Figs. 1(a) and 1(c). It is well known and easily observed that during drainage liquid flows through the films which swell with increasing liquid volume fraction [19,20]. Carrier and Colin [20] showed that films in foams have a minimal thickness, $h \sim 100$ nm, which increases linearly with ϵ. We quantify film-swelling behavior using a simple first-order approximation $h \propto (1 + h'\epsilon)$. This affords an ansatz for the stress that is the product of the Laplace pressure, T/R [21], and the shear across films, which is inversely proportional to film thickness,

$$\tau = g\frac{T}{R}(1 + h'\epsilon)^{-1}, \tag{7}$$

where the prefactor g and the film-swelling parameter h' may have a strain-rate dependence. Although the film shearing ansatz has one less free parameter than the film-stretching model, it yields a curve that falls on top of the measurements; see the black line in Fig. 3(b). The fitting error is 3 times smaller, $\langle\chi^2\rangle = 0.0017$, and the parameters are $g = 0.42 \pm 0.02$ and $h' = 30 \pm 4$.

To arrive at a constitutive relation accounting for both liquid content and strain rate, we perform several FDR experiments with various perfusion sequences and different angular velocities. For each ω, the film shearing parameters g and h' are determined by minimizing the $\langle\chi^2\rangle$ error. Figure 5(a) is a log-log plot showing power-law behavior $g \sim \omega^{0.2}$, which is in good agreement with Rodts' observations, Eq. (2), for shaving cream [7]. The film-swelling parameter h' exhibits a slow logarithmic decrease of about 30% over three decades in ω; see Fig. 5(b). We follow previous work and express the dimensionless form of the shear rate at the inner cylinder with the capillary number. Since the foam flows as a Bingham fluid and the gap is wide, the strain rate is $\dot{\gamma} = 2\omega/n$. Both the upper abscissas of Fig. 5 and the fits to the parameters are

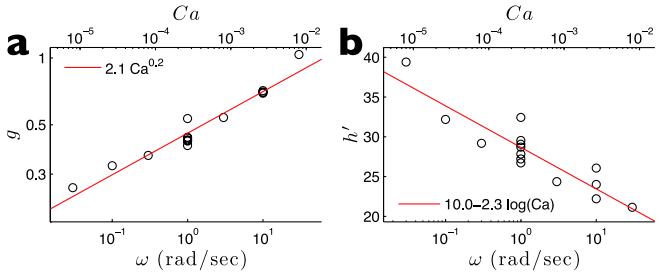

FIG. 5 (color online). Dependence of (a) strain-rate and (b) film-swelling terms from Eq. (7) on the rate of shear.

given in terms of the capillary number. Based upon the strain-rate dependence, we modify the ansatz equation (7), and obtain a constitutive relation

$$\tau = c\frac{T}{R}\left[\frac{\mathrm{Ca}^n}{1 + [k_1 - k_2 \log(\mathrm{Ca})]\epsilon}\right], \tag{8}$$

where $n = 0.2$, $c = 2.1$, $k_1 = 10$, and $k_2 = 2.3$. Preliminary results indicate that the parameters k_1 and k_2 change with bubble size. Thus similar to foam drainage, a more complete description would likely involve the interfacial mobility, which is the ratio of bubble size, bulk, and surface viscosity $\mu R/\mu_s$ [8,22,23].

We offer explanations for two trends involving the strain rate. The decrease of the film-swelling parameter h' with increasing Ca, which may be due to an increase in osmotic pressure with strain rates [24]. At greater strain rates the curvature of the channel walls increases, resulting in a larger Laplace (under)pressure and causing fluid to be sucked from the films. Second, shear-thinning is due to nonlinear processes involved in interfacial flows. Even for unsheared foams, the interfaces are swirling in a poorly understood, complex fashion [5,19,20,25]. The macroscopic shear results in opposing perturbations of the surface flows on opposite sides of the films, see Figs. 1(a) and 1(c), which leads to a lubrication flow across the films (i.e., film shearing).

In summary, we have developed the FDR procedure for performing various rheological tests on soap foams at fixed liquid volume fractions and bubble sizes. Our measurements of the continuous shearing stresses are in poor agreement with the film-stretching model [6]. We propose that film shearing is the dominant source of dissipation; thus, stresses depend inversely on film thickness where the films swell with increasing liquid volume fraction. We expect that FDR will prove useful for many different rheological experiments where controlled liquid content and bubble size are important, such as small-amplitude shearing, creep, and step strain. Improvements in measurements will advance rheological models as well as help in the general understanding of soft condensed matter.

We thank Proctor and Gamble for their support.

*Present address: Department of Physics, WPI, Worcester, MA 01609, USA.
sak@wpi.edu

[1] D. Weaire and S. Hutzler, *The Physics of Foam* (Oxford University Press, New York, 2000).
[2] P. Sollich, F. Lequeux, P. Hébraud, and M. E. Cates, Phys. Rev. Lett. **78**, 2020 (1997).
[3] R. Höhler and S. Cohen-Addad, J. Phys. Condens. Matter **17**, R1041 (2005).
[4] L. L. Schramm, *Emulsions, Foams, and Suspensions: Fundamentals and Applications* (John Wiley & Sons, New York, 2005).
[5] D. M. Buzza, C. Y. Lu, and M. E. Cates, J. Phys. II (France) **5**, 37 (1995).
[6] H. M. Princen and A. D. Kiss, J. Colloid Interface Sci. **128**, 176 (1989).
[7] S. Rodts, J. C. Baudes, and P. Coussot, Europhys. Lett. **69**, 636 (2005).
[8] N. Denkov, Colloids Surf. A **263**, 129 (2005).
[9] A. Saint-Jalmes and D. J. Durian, J. Rheol. (N.Y.) **43**, 1411 (1999).
[10] H. M. Princen, M. P. Aronson, and J. C. Moser, J. Colloid Interface Sci. **91**, 160 (1983).
[11] S. A. Khan and R. C. Armstrong, J. Non-Newtonian Fluid Mech. **22**, 1 (1986).
[12] L. W. Schwartz and H. M. Princen, J. Colloid Interface Sci. **118**, 201 (1987).
[13] S. A. Koehler, S. Hilgenfeldt, and H. A. Stone, Langmuir **16**, 6327 (2000).
[14] MATLAB's pdepe function was used for the simulations. The boundary conditions were $u = 0$ at the top, and $\epsilon = \epsilon_c$ at the bottom of the foam.
[15] S. A. Koehler, S. Hilgenfeldt, and H. A. Stone, Phys. Rev. Lett. **82**, 4232 (1999).
[16] P. Stevenson, Colloids Surf. A **305**, 1 (2007).
[17] G. Verbist, D. Weaire, and A. Kraynik, J. Phys. Condens. Matter **8**, 3715 (1996).
[18] D. J. Durian, Phys. Rev. E **55**, 1739 (1997).
[19] R. A. Leonard and R. Lemlich, AIChE J. **11**, 25 (1965).
[20] V. Carrier, S. Destouesse, and A. Colin, Phys. Rev. E **65**, 061404 (2002).
[21] T. G. Mason, M. D. Lacasse, G. S. Grest, D. Levine, J. Bibette, and D. A. Weitz, Phys. Rev. E **56**, 3150 (1997).
[22] S. A. Koehler, S. Hilgenfeldt, and H. A. Stone, J. Colloid Interface Sci. **276**, 420 (2004).
[23] S. A. Koehler, E. R. Weeks, S. Hilgenfeldt, and H. A. Stone, J. Colloid Interface Sci. **276**, 439 (2004).
[24] H. M. Princen, Langmuir **2**, 519 (1986).
[25] K. J. Mysels, K. Shinoda, and S. Frankel, *Soap Films: Studies of Their Thinning* (Pergamon, New York, 1973).